Interaction and coalescence of large bubbles rising in a thin gap

Sander G. Huisman,[1,2] Patricia Ern,[1,2] and Véronique Roig[1,2,*]

[1]*Université de Toulouse; INPT, UPS; IMFT (Institut de Mécanique des Fluides de Toulouse); Allée Camille Soula, F-31400 Toulouse, France*
[2]*CNRS, IMFT, F-31400 Toulouse, France*

We present accurate measurements of the relative motion and deformation of two large bubbles released consecutively in a quiescent liquid confined in a thin-gap cell. Although the second injected bubble was smaller, we observed that, in all cases, it accelerated and caught up with the leading bubble. This acceleration is related to the wake of the leading bubble, which also induces significant changes in the width and curvature of the trailing bubble. On the contrary, the velocity of the leading bubble is unaltered during the whole interaction and coalescence process. Shape adaptation of the two bubbles is observed just prior to coalescence. After pinch-off, the liquid film is drained at a constant velocity.

When two bubbles are rising in a quiescent fluid, the paths they follow are related to the perturbations they induce in the liquid and to their capacity to undergo deformation. In the tandem configuration (two bubbles rising along their lines of centers), the wake of the leading bubble is a powerful means to draw the bubbles together. This behavior is expected to promote coalescence, although escaping behavior may occur owing to the bubble's ability to deform or to lateral perturbations that may cause the bubbles to rotate and to line up horizontally [1,2]. Coalescence of a leading bubble with a trailing bubble is commonly observed in experimental high-Reynolds-number bubbly flows [3] but is currently not predicted by theoretical and numerical papers. Potential flow theory predicts that two bubbles rising in tandem will repel each other [4,5] with flow reversibility leading to the existence of a stagnation point between the two bubbles. Moreover, numerical simulations for nondeformable spherical bubbles at moderate-to-large Reynolds numbers predict that bubbles in line reach an equilibrium distance for which the repulsive potential effect balances the attractive viscous effect related to the vorticity produced at the bubble surface [1,6].

Presently, there is little quantitative information on the bubble's kinematics during their interaction and on its relationship with the bubble's deformation. The aim of this paper is to obtain a simultaneous characterization of the kinematics and deformation of two bubbles rising in tandem. For this purpose, we consider the interaction of two large bubbles rising freely in line in a vertical Hele-Shaw cell. The case of large bubbles is particularly interesting since their shapes are preserved by coalescence. The use of a Hele-Shaw cell has the advantage to constrain the motion and the deformation of the bubbles to the plane of the cell.

The motion of an isolated bubble rising in a quiescent liquid in a confined geometry has been studied in detail in Refs. [7–10]. Given the fixed width e of the cell, the equivalent diameter of the bubble is defined from the area A of the bubble in the plane of the cell $d = \sqrt{4A/\pi}$. Three nondimensional parameters governing the single-bubble problem may then be introduced, the Archimedes number $Ar = d\sqrt{gd}/\nu$, the Bond number $Bo = \rho g d^2/\sigma$, and the confinement ratio $e/d \ll 1$ (g being the gravity acceleration, ν being the liquid kinematic viscosity, ρ being the liquid density, and σ being the surface tension), the density and dynamic viscosity of the bubble being considered negligible relative to those of the liquid. For a given set of parameters, the resulting mean vertical velocity V_∞ of the bubble is used to define the Reynolds number $Re = V_\infty d/\nu$. Furthermore, the dimensionless quantity $\tilde{Re} = Re(e/d)^2$ compares the in-plane inertial time scale V_∞/d and the time scale for viscous diffusion in the gap e^2/ν. The classical Hele-Shaw regime corresponds to $\tilde{Re} \ll 1$, whereas inertial effects become predominant when $\tilde{Re} \gg 1$ [11]. In the present Brief Report, all the bubbles satisfy $6000 < Ar < 18\,000$, $Re \gg 1$, and $\tilde{Re} \gg 1$ and have the shape of a circular segment. When these bubbles are rising alone, we measure that their terminal velocities are given by the relation $Re = \sqrt{\frac{\pi}{2C_d}}\, Ar \simeq 0.42\, Ar$ or $V_\infty \simeq 0.42\sqrt{gd}$, indicating that their drag coefficients are, with a very good approximation, independent of the bubble size ($C_d \simeq 3\pi$) in agreement with Refs. [7,8]. Upstream of the bubble, the flow can be conveniently predicted by potential flow theory, whereas, the production of vorticity at the bubble surface results in the existence of a stationary wake as can be seen in Fig. 1. Moreover, the shear stresses at the walls impose a faster spatial decrease of the open wake in a Hele-Shaw cell than in an unbounded fluid, which is associated with the viscous length scale $l_\nu = V_\infty e^2/\nu$, namely, $u/V_\infty \simeq \exp\left[-10(y - y_R)/l_\nu\right]$, where y_R is the length of the recirculating wake measured from the bubble center $y_R \simeq 0.16 l_\nu$ [8]. At a distance of about $0.4 l_\nu$ ($\simeq 4d$ for $Ar \simeq 7000$), the liquid velocity in the open wake is already 10% of V_∞. Note that $l_\nu/d \sim 1/\sqrt{d}$ so that as Ar increases, the length of the recirculating wake decreases in terms of the bubble diameter ($y_R \simeq 1.6d$ for $Ar \simeq 7000$ and $\simeq 1.3d$ for $Ar \simeq 13\,500$).

The apparatus consists of two glass panes spaced 1-mm apart and filled with water. The cell has a width of 40 cm and a height of 80 cm, allowing us to visualize the entire process of interaction and coalescence, while making sure the bubbles are not affected by end effects. Gas injection is controlled manually by a combination of pressure reducing valves, stopcock valves, and dispensing needles. The bubbles are recorded using high-speed imaging, after which the
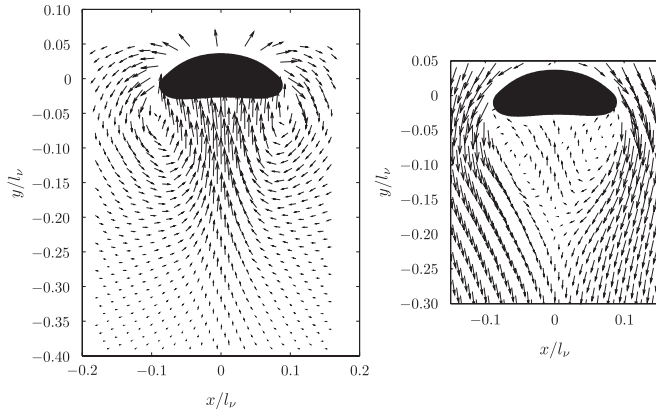
*roig@imft.fr

FIG. 1. Liquid velocity around an isolated large bubble obtained by particle image velocimetry (Ar = 7000, $V_\infty = 0.16$ m/s, $d = 1.5$ cm). Left, in the laboratory frame; right, focus on the recirculating wake in the bubble frame.

background is subtracted from the frames. The resulting frames are binarized, revealing the contours of the bubbles. From the contours, we obtain the kinematics and deformation characteristics of the bubbles.

We vary the injected gas volume for both bubbles and release them in rapid succession from a single capillary. We investigated the case where the second bubble is smaller than the first one. If the delay between the bubbles' injection is not too large, we observe that the trailing bubble catches up with the leading bubble, resulting in coalescence. Figure 2 provides an overview of this process. These experiments indicate that the suction effect provided by the wake of the leading bubble is sufficiently strong to accelerate the secondary bubble until it joins the first bubble. Moreover, this occurs even when the trailing bubble is smaller and has a smaller terminal velocity than the leading bubble, since the terminal velocity of an isolated bubble is proportional to $A^{1/4}$. Figure 2 also reveals that a strong deformation of the secondary bubble occurs when it is sufficiently close to the leading bubble. We now provide a detailed characterization of the whole interaction and
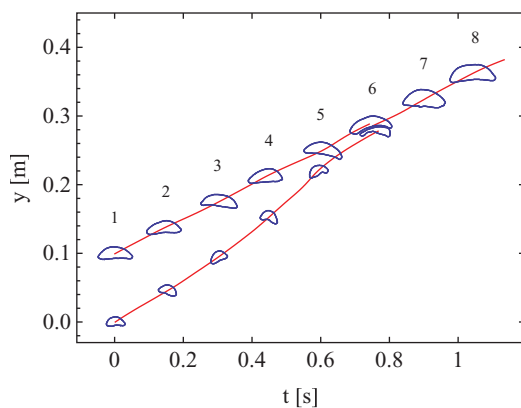

FIG. 2. (Color online) Overview of the trajectories of two coalescing bubbles (Ar$_1$ = 16 700 and Ar$_2$ = 8600). The trailing bubble is entrained in the wake of the leading bubble (1–5); the bubbles adapt their shapes (6) and coalesce forming a single bubble (7, 8).
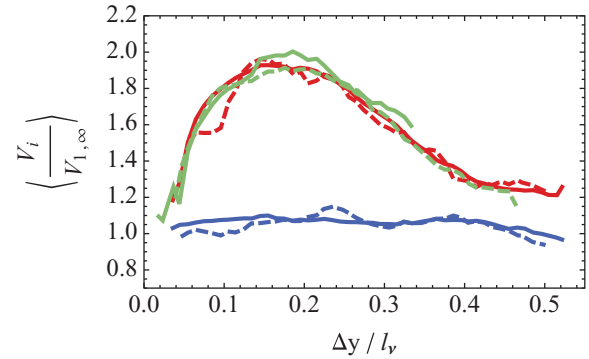

FIG. 3. (Color online) Vertical velocity of the trailing bubble (top lines) and of the leading bubble (bottom lines) normalized by the terminal velocity of an isolated bubble of the same size as the leading bubble. $\langle . \rangle$ denotes averaging over multiple experiments. (Darker solid lines) Results averaged over 40 experiments and (darker dashed lines) data from a single experiment (Ar$_1$ = 15 450 and Ar$_2$ = 8500). The green (light gray) curves compare two sets of experiments, both for $7500 < \text{Ar}_2 \leqslant 9000$ ($\langle \text{Ar}_2 \rangle = 8437$) and two different ranges of Ar$_1$, the dashed line for $11\,010 < \text{Ar}_1 < 12\,800$ ($\langle \text{Ar}_1 \rangle = 11\,806$), and the solid line for $15\,950 < \text{Ar}_1 < 17\,520$ ($\langle \text{Ar}_1 \rangle = 16\,685$).

coalescence process, in particular, the wake-induced relative motion of the two bubbles, their deformation when the bubbles are close enough, and finally, the thin liquid film drainage occurring after pinch-off of the two bubbles' interfaces.

The data presented are the mean of 40 experiments, performed over a range of Ar numbers ($10\,000 < \text{Ar}_1 < 17\,500$ and $6000 < \text{Ar}_2 < 10\,000$), where Ar$_2$/Ar$_1$ varies between 0.5 and 0.8 and where the indices 1 and 2 correspond to the leading and trailing bubbles, respectively. Figure 3 presents the instantaneous vertical velocities of the bubbles as a function of the distance between the centers of gravity of the bubbles. Both velocities are normalized with the terminal velocity of an isolated bubble of the same size as the leading bubble. On the abscissa, the distance between the centers of the bubbles is normalized using the viscous length scale l_ν. Figure 3 shows that the speed of the leading bubble is unaltered by the presence of the second bubble. This has also been observed in Ref. [12] for three-dimensional (3D) spherical caps, whereas, for small spherical bubbles, the velocity of both bubbles increases prior to coalescence [13]. Regarding the trailing bubble, Fig. 3 shows that it experiences a significant acceleration and then deceleration as it approaches the leading bubble. Thanks to the entrainment provided by the leading bubble's wake, the velocity of the trailing bubble is already 50% higher than its isolated speed and 20% higher than the speed of the leading bubble at $\Delta y \simeq 0.5 l_\nu$ (about four diameters away from the top bubble) and continues to increase while the trailing bubble is approaching the leading one. This acceleration phase was measured already in Ref. [12], but they carried out no measurement beyond $\Delta y / d_1 \approx 2.5$. When the distance between the bubbles is $\Delta y / l_\nu \approx 0.2$ ($\Delta y / d_1 \approx 2$), the velocity of the trailing bubble reaches a maximum, about two times faster than the speed of the leading bubble. This corresponds to frames 4 and 5 in Fig. 2. At that point, the trailing bubble is entering the attached recirculating wake of the leading bubble, and it starts to experience large deformations as described

later. This velocity is kept until $\Delta y/l_v \approx 0.1$ ($\Delta y/d_1 \approx 1$). For lower separation distances, the liquid between the two bubbles is pushed out, the bubbles become wider, and the trailing bubble slows down and adapts its velocity to the speed of the leading bubble. For trailing bubbles with $Ar_2 \approx 8440$, Fig. 3 also presents the evolution of their vertical velocity when the leading bubbles move either at $Ar_1 \approx 11\,810$ or at $Ar_1 \approx 16\,690$ [green curves (light gray top)]. We observe that all the curves superpose satisfactorily. The same result is obtained when fixing Ar_1 and considering two different sets of Ar_2. This result indicates that, in the ranges of Ar_1 and Ar_2 investigated here, the evolution of the velocity of the trailing bubble with the separation distance follows a unique master curve, provided the velocity is normalized with the velocity of the leading bubble and the separation distance with the viscous length scale associated with the leading bubble. This result fully reveals the crucial role of the wake of the leading bubble in the interaction process. Note that, for comparison, data from a single experiment is also presented. These data are not as smooth as the averaged velocity due to the shape oscillations of the body but also, in some cases, due to the possible lack of alignment of the two bubbles and associated slight horizontal motion.

During the entire process, the width and the curvature of the bubbles evolve. Figure 4 shows the width w and the curvature
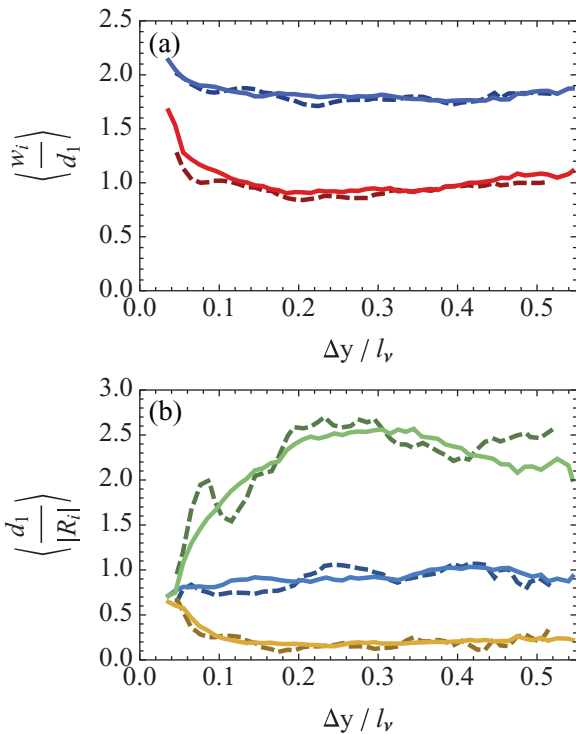

FIG. 4. (Color online) (a) Evolution of the normalized width of the bubbles during approach. Top and bottom lines correspond to the leading and trailing bubbles, respectively. (b) Curvature of the bubbles as a function of separation distance. Top, middle, and bottom lines correspond to the normalized curvature at the top of the trailing bubble, top of the leading bubble, and bottom of the leading bubble, respectively. (Solid lines) Results averaged over 40 experiments and (dashed lines) results from a single experiment ($Ar_1 = 15\,450$ and $Ar_2 = 8500$).

FIG. 5. Overview of different pairs of bubbles just prior to coalescence showing how the bubbles adapt their shapes to each other. Note that each pair of bubbles is shaped like a single big bubble ($Ar_1 \approx 11\,000$ and $Ar_2 \approx 7000$).

$1/R$ of the bubbles, normalized by the leading bubble diameter d_1 as a function of the separation distance. During the approach of the trailing bubble, from about four to two equivalent diameters apart (e.g., frames 1–4 in Fig. 2), the top bubble does not change its shape significantly. The constant velocity of the first bubble, thus, is associated with a constant front curvature as can be expected from potential flow theory [7]. The trailing bubble, on the contrary, experiences a pronounced change in shape. It first becomes narrower, which causes the curvature to increase as can be seen in Fig. 4. At $\Delta y/l_v \approx 0.2$, the width of the trailing bubble starts to increase, while its curvature and velocity start to decrease. As the bubble continues to approach the leading bubble, it becomes wider and slows down. In the final stage of the approach, the liquid between the two bubbles is pushed out, no immediate coalescence occurs, and the leading bubble adjusts itself in order to accommodate for the trailing bubble by becoming slightly wider (Fig. 4). The bubbles adapt the shape of their interface and match each other's curvature.

Figure 5 shows an overview of the bubbles just before they coalesce. Most of the liquid between the bubbles has been drained, and the shape of the two bubbles together closely resembles a single large bubble. In this situation, the drag of the pair is very close to the leading bubble drag ($C_d \simeq 3\pi$ and comparable velocities), whereas the drag of the pair is larger as long as the two bubbles have separated wakes. In addition, note that the bubbles are not always vertically aligned, despite being injected through the same nozzle, but in all cases, the trailing bubble is captured by the leading one.

The final stage of coalescence is the merge of the interfaces; the fluid between the two bubbles has thinned enough so that nonhydrodynamical forces trigger the film rupture [14]. The drainage has been observed to be in several forms, depending on the geometry of the bubbles as can be seen in Fig. 6. Film drainage can start at one end and then move across the entire
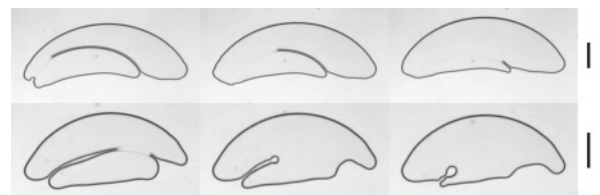

FIG. 6. Two sequences of film drainage. (Top three images) The liquid ligament is retracting at a constant velocity. (Bottom images) The film changes geometry halfway, and the fluid is collected in a rim. The scales on the right equal 1 cm.

bubble (see Fig. 6) or start in the middle upon which the fluid is evacuated in two directions. It is still an open question whether the fluid is drained partly in the films in between the bubble and the glass or in the sole plane of the cell. A thin liquid film exists between the moving bubbles and the walls. The thickness of this liquid film can be estimated by $h/e \approx \mathrm{Ca}^{2/3}/(1 + \mathrm{Ca}^{2/3})$ [8,15], where $\mathrm{Ca} = \rho \nu V_\infty / \sigma$ is the capillary number. For the largest bubbles of our experiments, this gives a film thickness of $h = 25\ \mu$m. In the experiments, we used demineralized water, and the scaling law giving the velocity of the isolated bubble ($\mathrm{Re} = 0.42\,\mathrm{Ar}$) suggests that the liquid speed in the films is negligible, indicating that a shear-free condition applies at the air-water interface of the thin films [7,8]. When the film separating the two bubbles is uniform (absence of a rim) as in the upper sequence of Fig. 6, we found the speed of the moving interface in the frame of reference of the bubble and along the curved film to be constant and about $v_d \simeq 1.65$ m/s. This measure was obtained with a time step of 0.5 ms over a length of the retracting film of 3 cm. Assuming that the drainage occurs in the plane of the cell and that the motion in the thin film is of Darcy type, i.e., that it results from a balance between pressure gradient and viscous friction at the walls, the mean drainage velocity in the gap (thickness e) is given by $v_d = \frac{e^2}{12\rho\nu}\frac{\partial P}{\partial s}$, s being the curvilinear abscissa along the film. The pressure gradient in the liquid film $\frac{\partial P}{\partial s}$ can be related to the difference in curvature along the 3D interface using Laplace's law. Considering that, in the gap, the bubble curvature is fixed everywhere by thickness e, the pressure gradient at leading order is driven by the change in the plane of the cell (over the length scale d) of the

bubble curvature due to the local merging. An order of magnitude of $\frac{\partial P}{\partial s}$, thus, is $\frac{1}{d}\frac{\sigma}{w}$, where the film thickness w is smaller than the radius of curvature of the bubble at the film exit ($w \ll d$, see Fig. 6). This leads to $v_d \simeq \frac{\sigma}{12\rho\nu}\frac{e^2}{wd}$, which is $O(1)$ m/s for $w \approx e$. A specific investigation should be carried out in the future to accurately measure the 3D geometry of the film and to verify that inertial effects can be neglected.

Accurate simultaneous measurements of the kinematics and of the deformation of two large bubbles rising in line allowed us to identify and to characterize the following different stages of interaction of the bubbles: (i) the trailing bubble is accelerated by the long-range wake of the primary bubble; (ii) the second bubble enters the recirculating wake of the leading bubble, undergoes horizontal contraction, and decelerates; (iii) the bubbles adapt their shape to each other, in particular, their curvatures are significantly modified; (iv) the shape of both bubbles together resembles a single bubble, and the liquid between the bubbles is squeezed out; and (v) the liquid film breaks, and the bubbles merge. The quantitative results presented here for each stage may provide a valuable test for future theoretical and computational papers on the road to predict bubbles' attraction and coalescence.

[1] Y. Hallez and D. Legendre, J. Fluid Mech. **673**, 406 (2011).

[2] J. B. W. Kok, Eur. J. Mech. B/Fluids **12**, 541 (1993).

[3] J. R. Vélez-Cordero, D. Sámano, P. Yue, J. J. Feng, and R. Zenit, J. Non-Newtonian Fluid Mech. **166**, 118 (2011).

[4] J. F. Harper, J. Fluid Mech. **41**, 751 (1970).

[5] J. B. W. Kok, Eur. J. Mech. B/Fluids **12**, 515 (1993).

[6] H. Yuan and A. Prosperetti, J. Fluid Mech. **278**, 325 (1994).

[7] R. Collins, J. Fluid Mech. **22**, 763 (1965).

[8] V. Roig, M. Roudet, F. Risso, and A.-M. Billet, J. Fluid Mech. (unpublished).

[9] M. Roudet, Ph.D. thesis, Institut National Polytechnique de Toulouse, France, 2008.

[10] S. Hosokawa and A. Tomiyama, J. Fluids Sci. Technol. **1**, 94 (2006).

[11] J. W. M. Bush and I. Eames, Int. J. Multiphase Flow **24**, 411 (1998).

[12] J. R. Crabtree and J. Bridgwater, Chem. Eng. Sci. **26**, 839 (1971).

[13] J. Katz and C. Meneveau, Int. J. Multiphase Flow **22**, 239 (1996).

[14] R. F. Probstein, *Physicochemical Hydrodynamics: An Introduction*, 2nd ed. (Wiley, New York, 1994).

[15] P. Aussillous and D. Quéré, Phys. Fluids **12**, 2367 (2000).